# Wintertime Blocking and Mountain Forcing of the Zonally-Averaged Flow: A Cross-Spectral Time Series Analysis of Observed Data

WERNER METZ

*Meteorological Institute, University of München, FRG*

(Manuscript received 20 March 1984, in final form 2 April 1985)

ABSTRACT

Nine winters of Northern Hemisphere observations are used for a statistical analysis of the relation between the mountain forcing of the zonally-averaged barotropic wind and blocking. Thereby, the temporal variability of the phenomenon "blocking" is expressed by a blocking index time series. It is demonstrated that the zonally averaged wind exhibits statistically significant negative anomalies at midlatitudes (40°N, 53°N) for the early blocking stage. The mountain drag is anomalously negative (corresponding to a slow-down of the zonal mean wind) at high (53°N, 70°N) and at middle (40°N, 53°N) latitudes. These significant negative mountain drag anomalies are found before the onset or at the very first stage of blocking. In terms of a signal-to-noise ratio, the strongest impact of the mountain drag on the zonal mean wind tendency occurs at the latitudes (30°N, 40°N), where the main mountain ranges of the earth are located.

## 1. Introduction

Blocking highs are most frequently observed in relatively confined regions of the northern Atlantic and Pacific Oceans. Consequently, a number of theoretical approaches to the blocking problem are via a geographically fixed forcing of the atmospheric flow. Such forcing mechanisms are, e.g., the regional anomalies of sea surface temperature (SSTA) or the interaction of the atmosphere with the earth's mountain ranges. The SSTA mechanism has been examined, e.g., by White and Clark (1975). Tung and Lindzen (1979) studied the combined effects of heat sources and mountains in the framework of a linear atmospheric model. Indirectly, i.e., via a three-dimensional time-mean basic state of a linear model, Frederiksen (1982) examined the impact of geographically fixed forcings on blocking. The mountain effect is the main forcing mechanism in the steady-state "multiple equilibria" blocking theory of Charney and DeVore (1979).

From the observational side, relatively little is known about the impact of regionally fixed forcing,—in particular, the mountain effect—on blocking. Hartjenstein (1984) suggested that a significant correlation exists between wintertime blocking episodes and the observed planetary midlatitude mountain-induced vertical energy flux. On the basis of a Charney and DeVore type model, Charney *et al.* (1981) showed that time-mean midlatitude longitudinal geopotential height profiles for a number of observed blocking cases are comparable to their model's results. Källen (1982) suggested that there may be some correlation between the zonally averaged mountain effect and blocking.

In view of the fact that the regionally fixed forcing is only one mechanism among a number of plausible mechanisms for sustaining blocks (for a review see Baines, 1983), further support from observed blocking episodes appear to be necessary. Because every case of blocking seems to be different in some respects from every other (Hartmann and Ghan, 1980), a statistical rather than a case study analysis appears to be the appropriate approach to the problem. Therefore, in this paper we use cross-spectral time series analysis to examine the relation between observed blocking episodes and mountain forcing. Our analysis is based upon the zonally averaged balance equation of the barotropic (i.e., vertically averaged) zonal wind component; i.e., the mountain effect considered in this paper is the mountain drag that acts upon the zonal mean flow. The mountain drag is computed from Northern Hemisphere observations.

The mountain drag is only one term that influences the wind balance. Therefore, it is necessary to make sure that this effect is not a second-order term. Because, in this paper, we apply cross-spectral analysis, it is natural to estimate the "strength" of the mountain effect in terms of the signal-to-noise ratio. This may be readily computed from the cross-spectrum of the mountain drag and the observed zonal wind tendency (cf. Section 3). Clearly, such an analysis provides only the normal, climatological impact of the mountain drag. We are aware, that this "strength" of the mountain effect may be different between blocking and nonblocking periods. However, in order to obtain the correct signal-to-noise ratio for the mountain effect under the condition that blocking prevails, one has to perform a multivariate analysis. Because of the great computational expense, this has not been undertaken. On the other hand, the

present paper is the first one which investigates the mountain effect in terms of cross-spectral time series analysis. Therefore, we feel that it will be justified to assume that at first approach the normal, climatological variance of the mountain will hold for blocking *and* nonblocking as well. This is supported by Hartmann and Ghan (1980) who indicated in the case of a local latitude-belt vorticity balance, that although there seem to exist differences, the order of magnitude of the terms is the same for blocking and for nonblocking.

To evaluate the statistical relationship between the mountain effect and blocking, we express temporal variability of the phenomenon "blocking" by a time series of a "blocking index." Such an index should reflect transient "bulk" characteristics of the observed Northern Hemisphere blocking activity. There are some hints that blocking is significantly related to such planetary "bulk" parameters. For example, it has been observed (Austin, 1980) that during blocking the longest planetary waves have anomalously high amplitudes. Or, the eddy kinetic energy of an extratropical latitude belt seems to undergo a systematic maximum during an early blocking stage, while at the same time the zonal kinetic energy tends to be minimal (Schilling, 1985; Hansen and Chen, 1984). In this paper, we apply, in particular, two different blocking indices, one of which is based on the aforementioned energy arguments (Schilling, 1985). The other index goes back to Hartjenstein (1984) who constructed a "synthetic blocking time series" from information on calendar dates of observed blocking events.

In Section 2, we give definitions and describe the data basis for our computations. There, we also outline the method for evaluating wind and mountain drag. The wintertime cross-spectrum of mountain drag and wind change is presented in Section 3. This section should help in estimating the importance of mountain drag for the zonal wind balance. In Section 4, the blocking indices are discussed and the results for the cross-spectral analyses concerning the relation between blocking and the mountain effect are presented. The results are discussed in Section 5, where we also give some comments on the barotropic blocking theory of Charney and DeVore.

## 2. Definitions and computational methods

### *a. Zonal mean balance of vertically averaged wind*

In this study the mountain effect is considered in the framework of the balance of the barotropic zonal wind in a closed latitude belt of unit width. Using $\sigma = p/p_s$ ($p_s$ is surface pressure) vertical coordinates this equation reads

$$\partial[\hat{u}]/\partial t = -1/(a\cos\varphi)\partial([uv]\cos\varphi)/\partial\varphi + f[\hat{v}] + g/(p_0 a\cos\varphi)[h\partial p_s/\partial\lambda] + g/p_0[\tau_{\lambda s}] \quad (1)$$

where

$$[(\ )] = \frac{1}{2\pi}\int_0^{2\pi}(\ )d\lambda \text{ and } (\hat{}\ ) = \frac{1}{p_0}\int_0^1(\ )p_s d\sigma;$$

$h$ is orography, $\tau_{\lambda s}$ is the zonal component of the surface stress, $f = 2\Omega\sin\varphi$ and $p_0 = 1000$ mb. For convenience we have written all the terms in (1) as accelerations; multiplication with the mass of a vertical air column ($p_0/g$) yields the zonally averaged momentum balance [the relative angular momentum balance is obtained by multiplying (1) with the distance from the earth's axis of rotation $a\cos\varphi$].

We find from (1) that $[\hat{u}]$ may change due to the impact of meridional momentum fluxes, the Coriolis effect, the mountain forcing and of the surface stress. In the present paper we deal only with the third term in (1), e.g., the drag (or push) that is exerted on the atmosphere by the earth's topography:

$$m_d = g/(p_0 a\cos\varphi)[h\partial p_s/\partial\lambda]. \quad (2)$$

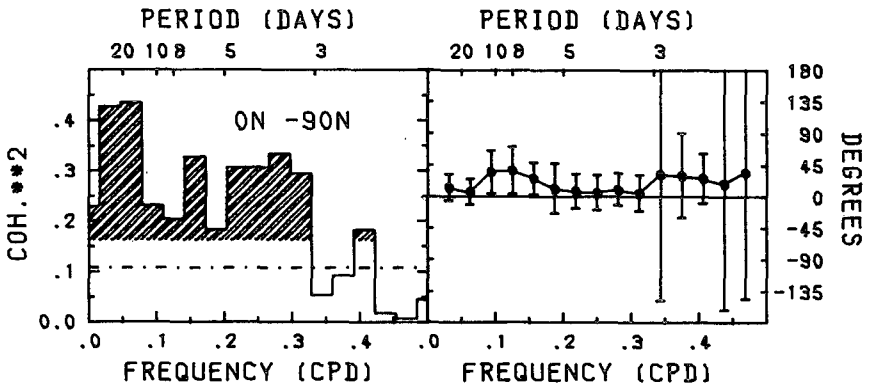


FIG. 1. The squared coherency (left) and phase (right) spectra for $D(0°–90°)$ and $dU(0°–90°)/dt$. The spectral estimates are based upon 54 dof. The 95% significance level for the squared coherency (dashed–dotted). Estimates exceeding the 99% significance level (hatched). Vertical bars in phase spectrum denote a 95% confidence interval.

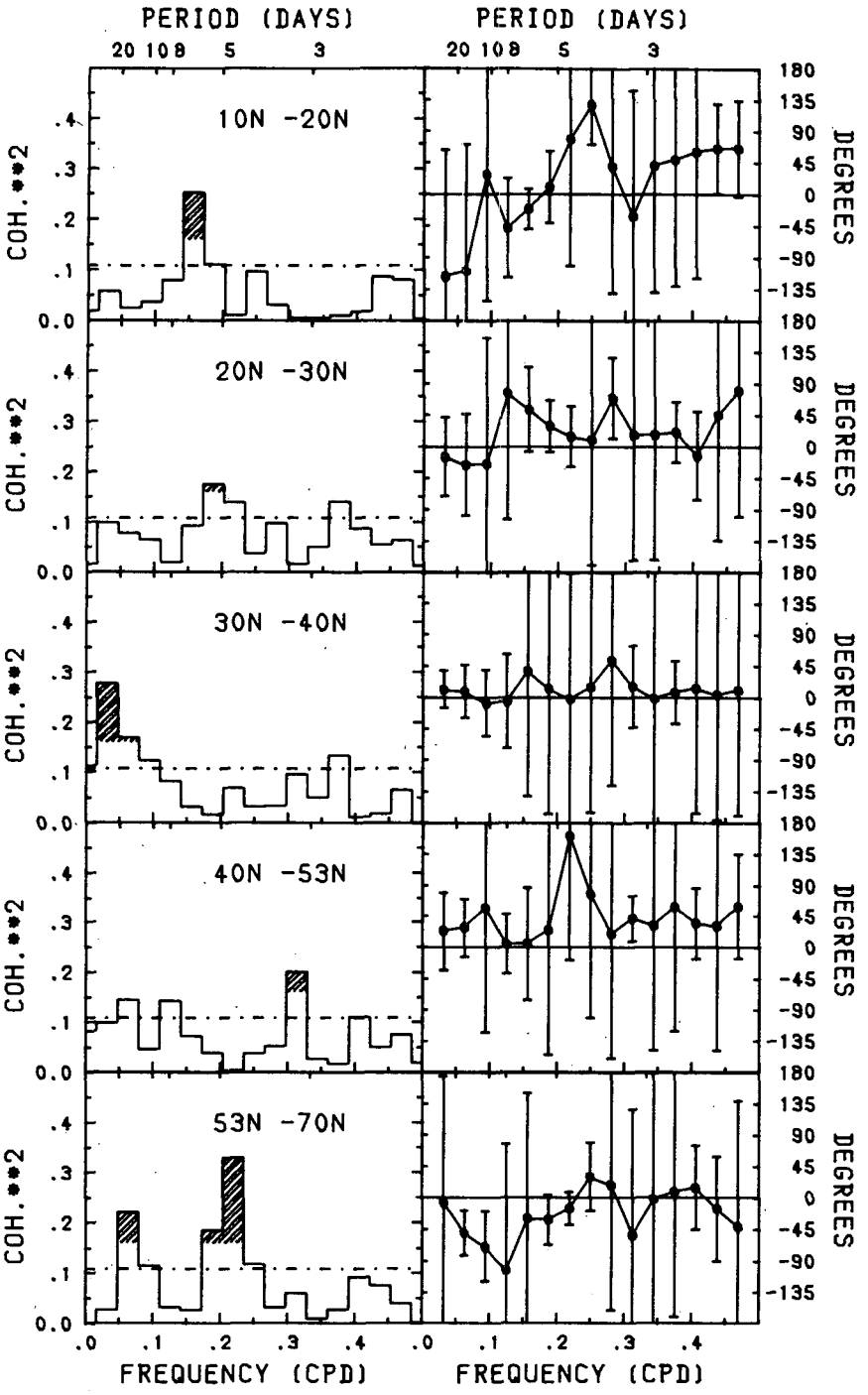


FIG. 2. As in Fig. 1 but for indicated latitude belts.

A positive drag causes an acceleration of the zonal mean wind. The square brackets in (2) represent the sum of the east–west pressure differences across all mountain ranges along an entire latitude circle. It should be mentioned that this definition is a little different from the quasi-geostrophic mountain effect which measures basically the mountain induced divergence. Monthly mean values of the zonal mean mountain effect in the Northern Hemisphere planetary angular momentum balance have been studied by White (1949), Newton (1971), and Oort and Bowman (1974).

TABLE 1. The coherency and correlation coefficient between mountain drag at indicated latitude belts. $K^2$: The components of squared coherency at frequency $f_i$ = 1/32 to 3/32 cpd. Values exceeding the 99% significance level (0.16) are in italic. $r_{xy}(l)$: The value ($r$) and lag ($l$, days) of the main peak of the lagged correlation coefficient, 99% significant values are in italic.

| | | $D$(40°–53°) | $D$(53°–70°) |
|---|---|---|---|
| | | 1/32 2/32 3/32 | 1/32 2/32 3/32 |
| $D$(30°–40°) | $K^2$ | *0.372 0.374 0.470* | *0.353 0.299* 0.070 |
| | $r_{xy}(l)$ | *0.51(0)* | *−0.23(−3)* |
| $D$(40°–53°) | $K^2$ | | *0.207 0.347 0.182* |
| | $r_{xy}(l)$ | | *0.32(0)* |

### b. Computation of wind and mountain drag

Our basic data set is the daily 0000 GMT Deutscher Wetterdienst (DWD) routine analyses of Northern Hemisphere geopotential heights and temperatures at 100, 200, 300, 500, 700 and 850 mb and the sea-level pressure $p_{sl}$ for a period of ten years from 1967 to 1976. The analyses were transformed to surface spherical harmonics coefficients. Thereby it was assumed that height and temperature were symmetric with respect to the equator. The spherical harmonics transform was triangularly truncated at zonal wavenumber $m = 15$. It comprises only symmetric modes (136 real coefficients). See Speth and Kirk (1981) for further details. The topographic heights of earth's surface are taken from the high resolution U.S. Navy terrain height data set which was kindly supplied to us by the European Centre for Medium Range Weather Forecasts.

We computed time series of daily latitude belt averages of $[\hat{u}]$ and $m_d$:

$$U(\varphi_1, \varphi_2) = (\sin\varphi_2 - \sin\varphi_1)^{-1} \int_{\varphi_1}^{\varphi_2} [\hat{u}] \cos\varphi \, d\varphi \quad (3a)$$

$$D(\varphi_1, \varphi_2) = (\sin\varphi_2 - \sin\varphi_1)^{-1} \int_{\varphi_1}^{\varphi_2} m_d \cos\varphi \, d\varphi. \quad (3b)$$

The wind was calculated by applying the geostrophic approximation. Following the method of Lorenz (1979), we solved the linear balance equation on the sphere in terms of spherical harmonics coefficients. As the geopotential height coefficients comprised only of symmetric modes, we obtained only antisymmetric modes for the streamfunction coefficients. The barotropic part of the zonally averaged wind may be recovered from the vertically averaged streamfunction coefficients $\hat{\psi}_n{}^m$ via

$$[\hat{u}](\varphi) = -1/[a(1-\mu^2)^{1/2}] \sum_{k=1}^{K} (4k-1)^{1/2}(2k-1) \times \{P^0_{2k-2}(\mu) - \mu P^0_{2k-1}(\mu)\}\hat{\psi}^0_{2k-1} \quad (4)$$

where $\mu = \sin\varphi$ and $K = 7$. Please note, that the superrotation $U_s(\varphi)$ can be easily obtained by truncating the expansion in (4) after $k = 1$ [$U_s(\varphi) = -(3)^{1/2}\psi_1{}^0 \times \cos\varphi = U_0 \cos\varphi$].

The mountain drag $m_d$ was evaluated in a latitude–longitude grid with 5° longitude and 2° latitude increments. The grid covers the Northern Hemisphere from 2°N through 88°N. Grid-point values of geopotential height and temperature are recovered from the spherical harmonics coefficients. Over land areas, the local surface pressure $p_s$ is computed by means of the barometric height formula. Over the sea, the recovered sea-level pressure $p_{sl}$ is used. Thus, along the same latitude belt, $p_s$ varies over rather a large range from 500 mb in the highest mountain regions to 1000 mb over the sea. Therefore, the derivation by longitude that appears in formula (2) had to be evaluated with great care. For that purpose we fitted a cubic spline data smoother function to the $p_{sl}$-values along each latitude belt. By analytical differentiation of the spline function we then obtained sufficiently smooth estimates of the longitudinal gradients. These estimates entered the evaluation of $m_d$ according to (2) as a function of latitude and time.

## 3. The wintertime cross-spectrum of mountain drag and zonal wind change

In this section we estimate the order of magnitude of the mountain drag in the balance equation (1). This is done in terms of the signal-to-noise ratio. As discussed in the Introduction, we assume that this estimate may hold for blocking and nonblocking periods as well. At the same time the normal wintertime correlation between mountain drag and wind change is investigated at the same latitude and between different latitudes. Wintertime anomalies of mountain drag and zonal wind were evaluated according to (3a, b) for the nine winters from 1967/68 to 1975/76. Then, cross-spectra of the anomaly time series are computed. The data set used for the evaluations has been described in Section 2b.

Let us commence by looking at Northern Hemisphere averages. In Fig. 1 the wintertime squared coherency $K^2(f_i)$ and phase spectra $F(f_i)$ [viz. (A2), (A3)]

TABLE 2. The coherency and correlation coefficient between zonal mean wind at indicated latitude belts. (As in Table 1.)

| | | $U$(40°–53°) | $U$(53°–70°) |
|---|---|---|---|
| | | 1/32 2/32 3/32 | 1/32 2/32 3/32 |
| $U$(30°–40°) | $K^2$ | 0.023 0.050 0.030 | 0.122 *0.347 0.643* |
| | $r_{xy}(l)$ | 0.08(6) | *−0.36(0)* |
| $U$(40°–53°) | $K^2$ | | 0.011 0.065 0.061 |
| | $r_{xy}(l)$ | | −0.11(0) |

TABLE 3. The coherency and correlation coefficient between mountain drag and zonal mean wind tendency at indicated latitude belts. (As in Table 1.)

| | | $dU(30°–40°)/dt$ | $dU(40°–53°)/dt$ | $dU(53°–70°)/dt$ |
|---|---|---|---|---|
| | | 1/32 2/32 3/32 | 1/32 2/32 3/32 | 1/32 2/32 3/32 |
| $D(30°–40°)$ | $K^2$ | *0.279 0.170* 0.125 | *0.161 0.273* 0.141 | 0.041 0.030 0.058 |
| | $r_{xy}(l)$ | *0.27(0)* | *0.24(0)* | −0.11(1) |
| $D(40°–53°)$ | $K^2$ | 0.086 *0.168* 0.151 | 0.099 0.145 0.046 | *0.193 0.202* 0.102 |
| | $r_{xy}(l)$ | *0.15(0)* | *0.20(0)* | *0.22(4)* |
| $D(53°–70°)$ | $K^2$ | 0.112 *0.166* 0.066 | 0.147 0.110 0.011 | 0.027 *0.221* 0.117 |
| | $r_{xy}(l)$ | *0.17(−3)* | *0.18(−1)* | *0.18(1)* |

are shown for the hemispheric mountain drag $D'(0°, 90°)$ and wind tendency $dU'(0°, 90°)/dt$ anomalies [viz. (A1)]; for convenience the prime and degrees are dropped in the following. We observe highly significant coherencies at virtually all frequency bands. Thereby, the test statistic for the squared coherency (A5) is 0.11 with an error probability of 5%, respectively, 0.16 with an error probability of 1%. Note, however, that the largest coherencies occur at the low-frequency tail of the spectrum, i.e., at periods of 64 days to 12 days. A

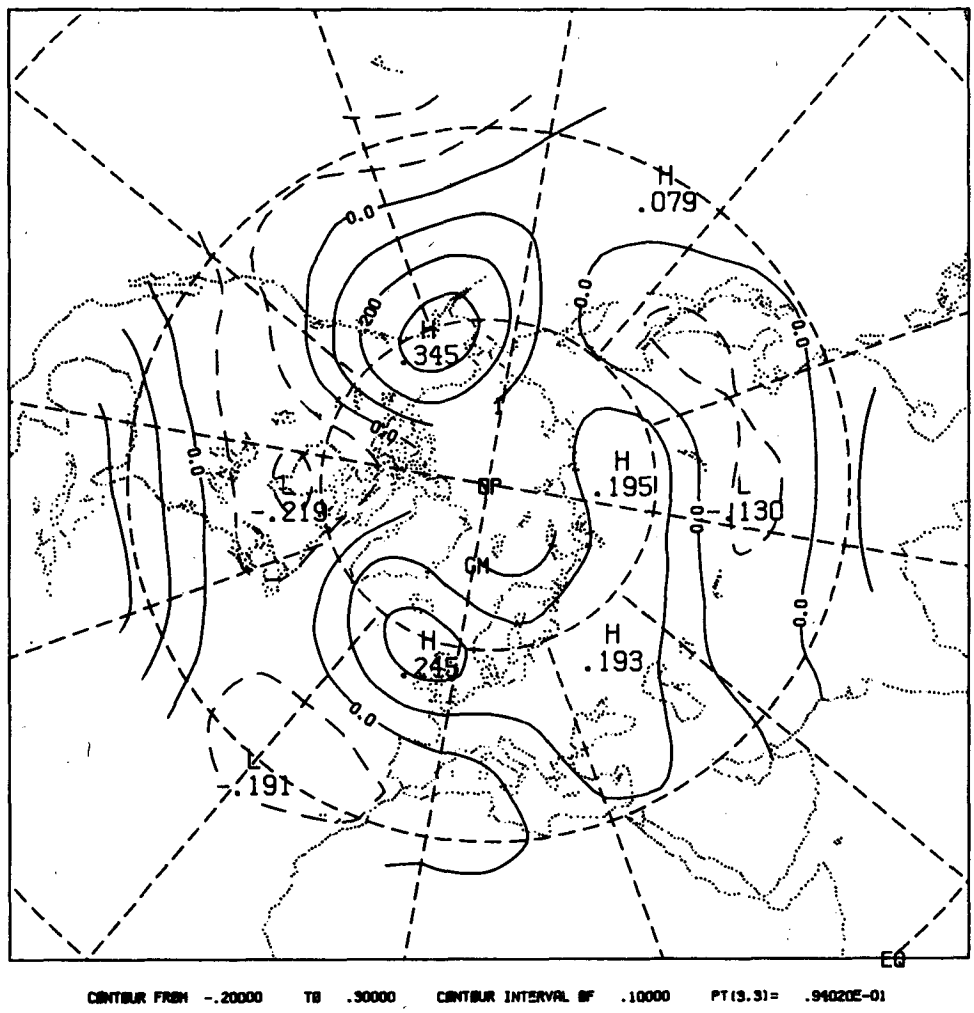


FIG. 3. The low-frequency correlation of blocking index *BS* leading the local wintertime 500 mb streamfunction anomalies by two days. Spacing of contour intervals is 0.1; negative contours (dashed); 99% significance level is 0.15. (See text.)

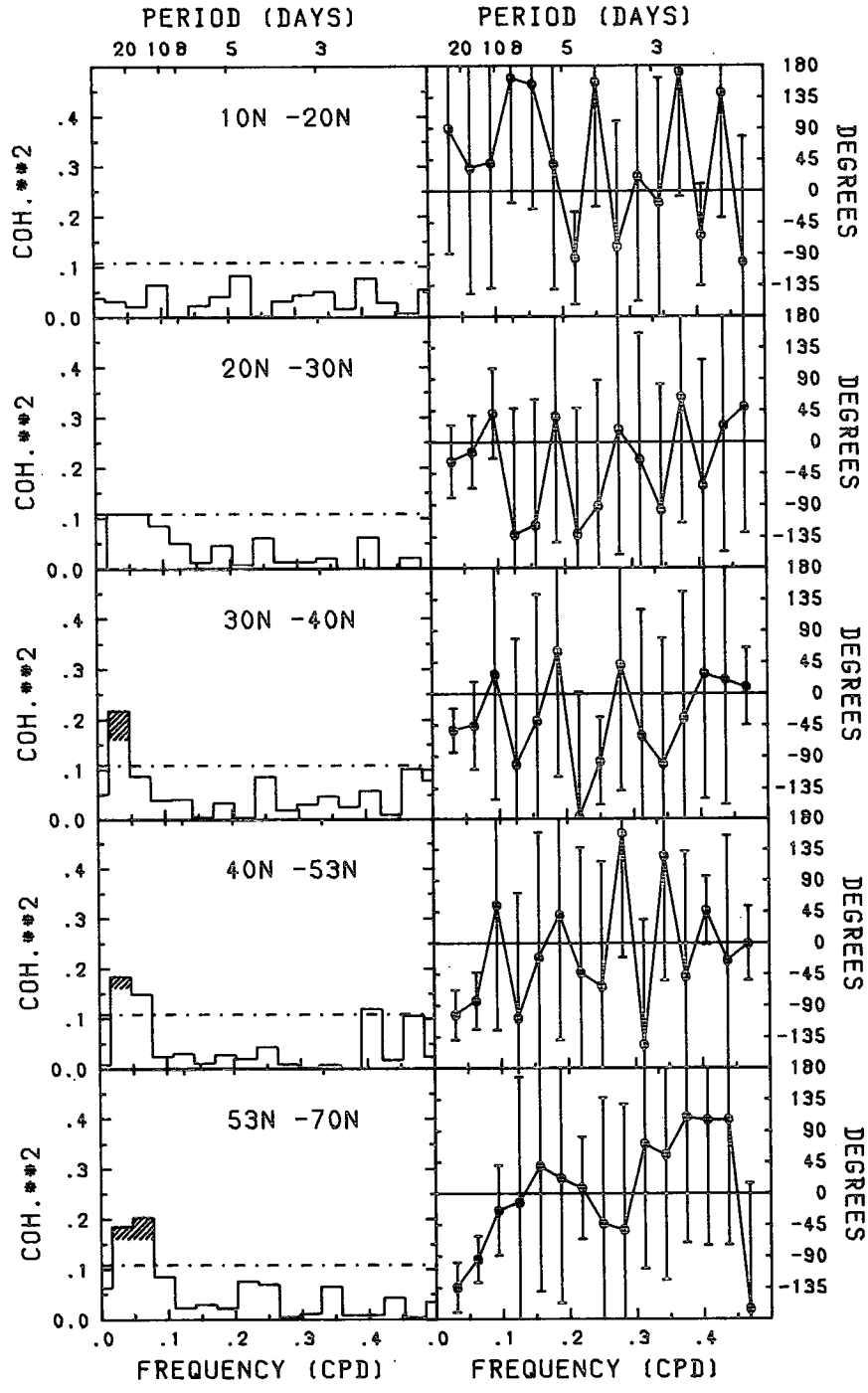


FIG. 4. The coherency and phase spectrum for blocking index *BS* and indicated latitude belt averages of mountain drag. (As in Fig. 1.)

close correlation between the hemispheric mountain drag and wind change can be seen from the phase spectrum. The 95% confidence intervals for the phases points towards an in-phase ($F = 0$) relationship between the two variables. For convenience, we have also computed the correlation coefficient $r(l)$ [cf. (A4)] at lags $l$ from $-10$ days $\leqslant l \leqslant 10$ days. We have a very pronounced peak at $r(0) = 0.46$ (the 99% significance level is 0.11).

It is well-known that $K^2(f_i)/[1 - K^2(f_i)]$ measures the signal-to-noise ratio at frequency $f_i$ (e.g., Jenkins and Watts, 1968). We have $K^2 = 0.43$ at $f = 1/32$,

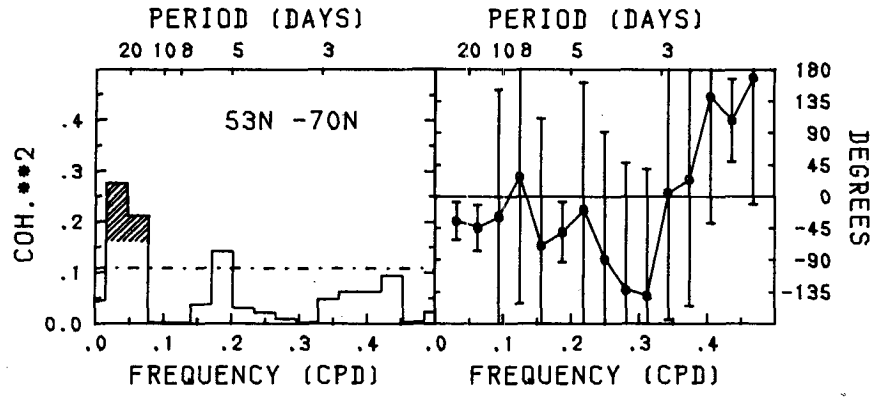


FIG. 5. As in Fig. 4 but for blocking index $BL$ and mountain drag $D(53°, 70°)$.

2/32; thus one obtains a signal-to-noise ratio of 0.75. This means that the low-frequency variance of the wind change which may be explained linearly by the mountain effect is 75% of the variance due to the noise processes in the system [i.e., the remaining terms in (1)]. At synoptic-scale frequencies (periods 5–3 days), one obtains a signal-to-noise ratio of typically 0.45.

Thus, the hemispheric zonal wind balance is strongly influenced by the mountain effect. Now, obviously, the topography of the earth's surface is not homogeneously distributed with latitude. Therefore, we will now examine the contributions of the mountain forcing that results from different latitude belts. Because the mountain drag is a very noisy quantity, it is reasonable to consider not too small latitude intervals. We have selected the latitude belts (10, 20), (20, 30), (30, 40), (40, 53) and (53, 70) which all represent approximately the same area on the Northern Hemisphere.

The squared coherency and phase spectra for the latitude belts are displayed in Fig. 2. In general, we have smaller coherency values for the latitude belts than for the hemispheric case. Because blocking is generally associated with slow variations of the atmospheric flow, we concentrate upon the low-frequency part of the spectrum which covers periods from 64 to 9 days ($f_i$ = 1/32, 2/32 and 3/32 cpd). At those frequencies we observe highly significant coherencies at the belt (30, 40), i.e., where the major elevations of the earth's topography (Himalaya, Rockies) are located. In terms of the signal-to-noise ratio the low-frequency power of the wind change, explained by the mountain drag, is about 30%. The phase spectrum suggests $F = 0$ at low frequencies which parallels the phase spectrum for the hemispheric case. For this case the correlation coefficient has its maximum at $r(0) = 0.25$. We find also significant low-frequency coherencies at high latitudes (53, 70). Here, we have significantly negative phases, suggesting a lag of the wind change after the mountain forcing. This comes out also in the correlation coefficient which exhibits peaks when the wind change lags the mountain drag by one day [$r(1) = 0.18$]. At low latitudes, there are no low-frequency coherencies.

Large-scale atmospheric flow systems with a broad latitudinal extent may lead to a significant correlation among the latitude belt averages of $m_d$. The same may also hold for the latitude belt averages of $[\hat{u}]$. To examine this possibility we have performed cross-spectral analyses between the same variables but at different latitudes. In Table 1 the low-frequency tail of the squared coherency spectrum is presented for the mountain drag at different latitudes. In addition, we also give the main peak of the correlation $r(l)$. Values in italics are significant with 1% error probability. We observe significant coherencies for the analyses between adjacent latitude belts. The strongest correlation is between $D(30, 40)$ and $D(40, 53)$. We have also large coherencies between $D(30, 40)$ and the high latitude belt mountain drag $D(53, 70)$. The latter gives a negative correlation (−0.23) at a lag of −3 days. The correlation between latitude belt averages of $U$ is given in Table 2. Of interest is the fact that we find no correlation between $U(30, 40)$ and $U(40, 53)$, but very large coherencies between $U(30, 40)$ and $U(53, 70)$. The phase spectrum (not shown) indicates a significant out-of-phase relationship and the correlation coefficient exhibits a pronounced peak at $r(0) = -0.36$. Such a strong out-of-phase coupling between the zonal average wind at high and lower middle latitudes can also be seen in the pattern for the second EOF of the zonal average wind, as communicated recently by Branstator (1984).

In view of the fact that energy propagation on the sphere tends to follow great circle routes, one should also consider the possibility of a significant correlation between the mountain forcing and the wind at different latitudes. The results of this analysis are presented in Table 3. Clearly, the low-frequency part of the spectra exhibit two dominant correlations between different latitude belts. First, the mountain drag at (30, 40) has significant coherencies with the wind change at (40, 53), where the maximum correlation is at $r(0) = 0.24$.

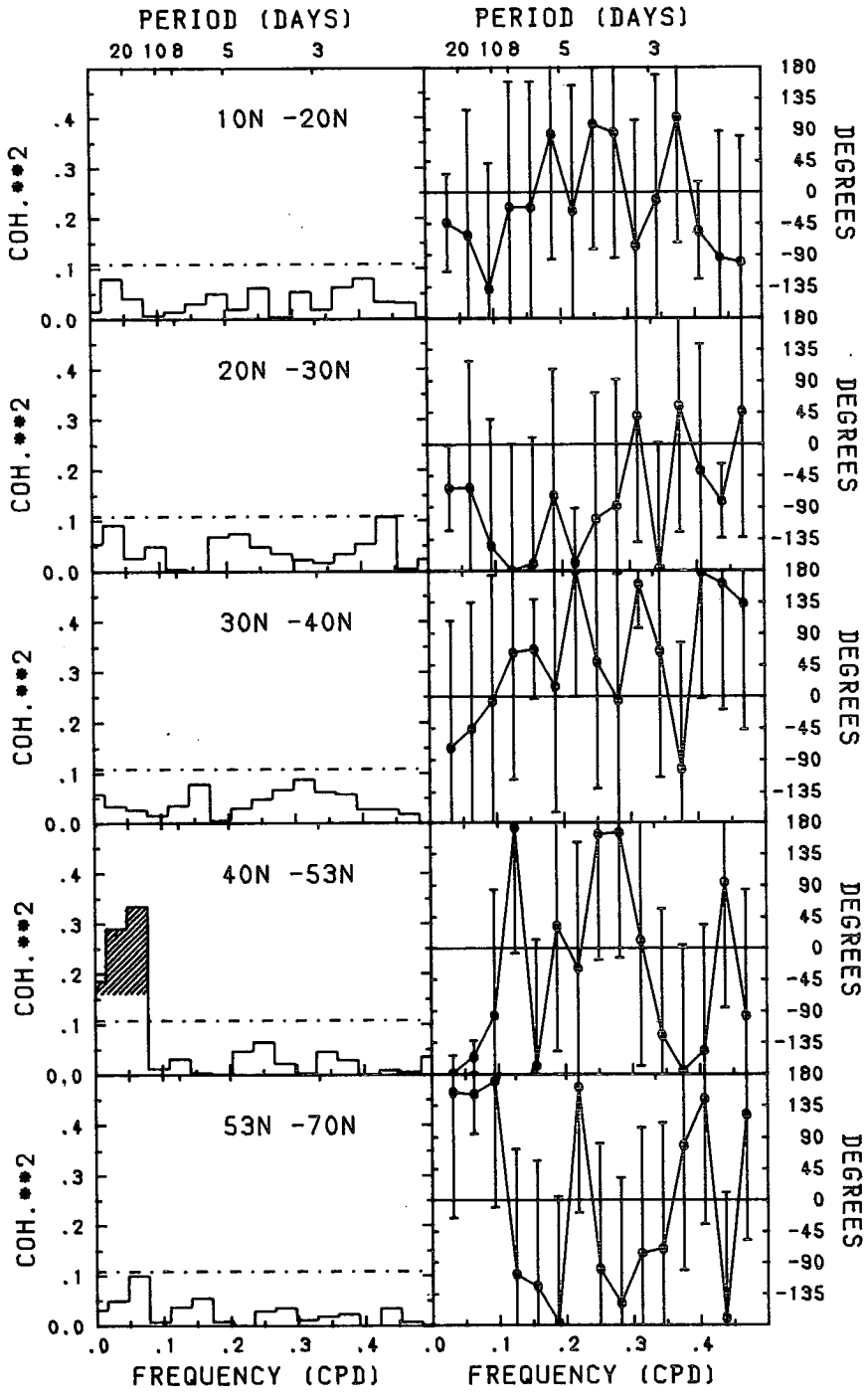


FIG. 6. As in Fig. 4 but for blocking index *BS* and indicated latitude belt averages of zonal mean wind.

Please note that we did not find significant coherencies between both variables at the same (40, 53) belt itself. The other significant correlation is between $D(40, 53)$ and the wind change at (53, 70). In that case, there is a lag of four days of the wind change after $D(40, 53)$. The above discussed coupling between the wind anomalies at (30, 40) and (53, 70) may be recognized also in Table 3 for the analysis with $D(40, 53)$ and $D(53, 70)$, but not for $D(30, 40)$.

Thus it appears that the main in-phase contribution to the hemispheric low-frequency correlation between $D(0, 90)$ and $dU(0, 90)/dt$ originates from the (30, 40)

TABLE 4. The coherency and correlation coefficient between blocking indices *BL*, *B7*, *BS* and the hemispheric mean mountain drag, respectively, the superrotation. (As in Table 1.)

| | | *BL* | *B7* | *BS* |
|---|---|---|---|---|
| | | 1/32 2/32 3/32 | 1/32 2/32 3/32 | 1/32 2/32 3/32 |
| $D(0°–90°)$ | $K^2$ | *0.295* 0.097 0.015 | *0.235* 0.057 0.050 | *0.234 0.197* 0.078 |
| | $r_{xy}(l)$ | *0.20(−1)* | *−0.19(6)* | *−0.27(6)* |
| $U(0°–90°)$ | $K^2$ | 0.046 0.011 0.072 | 0.102 0.034 0.029 | 0.101 *0.200* 0.060 |
| | $r_{xy}(l)$ | −.08(2) | −0.18(4) | *−0.28(1)* |

latitude belt. On the other hand, the mountain drag at high latitudes has also significant low-frequency coherencies with the wind change, but the correlation seems to occur at a significant lag between the two time series.

## 4. Statistical relation between blocking and mountain effect

### a. *Blocking indices*

Schilling (1985) has combined observed planetary energy parameters to a dimensionless number

$$BS(t) = K_e L_c^2/(K_T L_{\text{crit}}^2) \tag{5}$$

where $K_e$ is the eddy kinetic energy, $K_T$ the kinetic energy of the vertical shear of the zonal mean flow, $L_c$ is a typical length scale and $L_{\text{crit}}$ is the Rossby radius of deformation. All parameters were evaluated for a closed latitude belt. This planetary blocking index *BS* reflects virtually the characteristic behavior of large-scale energetics with respect to blocking episodes (cf. the Introduction, also Hansen and Chen, 1984). A statistical analysis of ten years of observed data shows that *BS*(*t*) (*Bl* in Schilling's notation) responds correctly for about 70% of all blocking cases. To give additional evidence of the performance of *BS*(*t*), we have computed the low-frequency (see A4) wintertime correlation coefficient (576 days) between *BS*(*t*) and the local (10° by 5°) detrended 500 mb streamfunction gridpoint anomalies [cf. (A1)]. Figure 3 shows the correlation for *BS*(*t*) leading the anomalies of the streamfunction by two days. Clearly, the most striking features are the dipoles in the Atlantic and Pacific Oceans, respectively. We have areas of high positive correlation at 20°W, 60°N and at 150°W, 60°N, i.e. just in the regions where blocking anticyclones are most frequently observed. However, it is most interesting to note that we have also significant correlations at latitudes where normally no blocks are observed. Thus, a negative correlation appears south of the positive maxima where, one often observes lows that accompany the blocking high. Significant negative correlations are found also over the Canadian shield. The center of northern Soviet Union blocking (Dole, 1982) may be identified. Let us emphasize that we observed maximal correlation if *BS* leads the local height (streamfunction) anomalies. This means, that the *BS* index attains its maximum at the very early stage of a blocking episode, before the height anomaly is fully developed.

In addition to *BS*(*t*), we apply a blocking index derived from the calendar dates of observed blocking episodes. It has been developed by Hartjenstein (1984) who adopted the blocking episodes from a catalogue of blocking (Treidl *et al.*, 1981). Let $s_j$ denote the time of the onset and $l_j$ the duration in days of the $j$th block. Then, the blocking index *BL*(*t*) is defined as

$$BL(t) = \sum_{j=1}^{J} w_j(t - s_j - l_j/2) \tag{6}$$

TABLE 5. The coherency and correlation coefficent between blocking index BS and mountain drag, respectively, zonal wind tendency at indicated latitudes. (As in Table 1.)

| | | *D*(30–40°) | *D*(40–53°) | *D*(53–70°) |
|---|---|---|---|---|
| *x* | | 1/32 2/32 3/32 | 1/32 2/32 3/32 | 1/32 2/32 3/32 |
| *BS* | $K^2$ | *0.219* 0.089 0.039 | *0.185* 0.150 0.025 | *0.186 0.204* 0.081 |
| | $r_{xy}(l)$ | *0.20(2)* | *−0.24(−6)* | *−0.28(−4)* |
| | | *dU*(30–40°)/*dt* | *dU*(40–53°)/*dt* | *dU*(53–70°)/*dt* |
| | | 1/32 2/32 3/32 | 1/32 2/32 3/32 | 1/32 2/32 3/32 |
| *BS* | $K^2$ | 0.035 0.026 0.015 | *0.291 0.336* 0.011 | 0.050 0.100 0.001 |
| | $r_{xy}(l)$ | −0.18(6) | *−0.56(0)* | −0.27(1) |

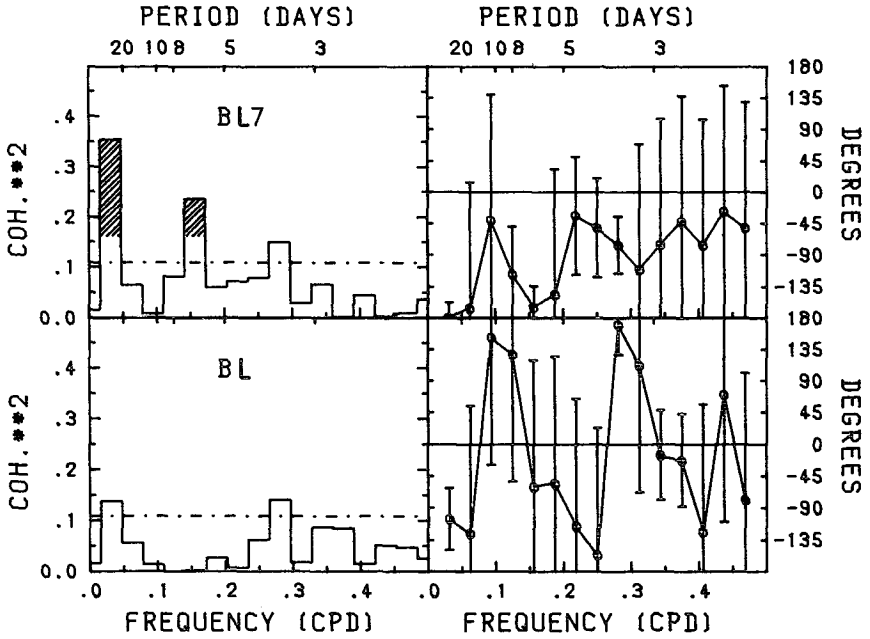


FIG. 7. As in Fig. 6 but for blocking index $B7$ (above), respectively, $BL$ (below) and zonal mean wind $U(40°, 53°)$.

where

$$w_j(d) = \begin{cases} \sin(\pi/l_j(d + l_j/2)) & |d| \leq l_j/2 \\ 0 & |d| > l_j/2 \end{cases}$$

and $J(=197)$ the number of blocks observed in 1967–76. Each block is represented by a half-sine signal with amplitude 1 centered on the middle of the block. In the following, it is referred to as "mature-stage" blocking index. From the behavior of local geopotential height anomalies (Dole, 1982), one might expect that the shape of the blocking signal $w_j(d)$ should look more like a "box-car" than a half-sine. However, the observations indicate (e.g., Hansen and Chen, 1984) that bulk parameters, e.g., the large-scale eddy kinetic energy may behave smoother than local geopotential height anomalies. A second reason for choosing a smooth shape of $BL(t)$ is that unwanted Gibbs-effects in the Fourier transformations are avoided.

It is an evident shortcoming of $BL(t)$ that it cannot distinguish between blocks of different intensities and the same durations, nor its scale or geographical distribution. Furthermore, $BL(t)$ is centered on the mature stage of a block and thus not particularly suitable to reflect the observed early stage energy fluxes. To overcome this deficiency we use a somewhat modified version of $BL(t)$. This index, $B7(t)$, is focused on the first seven days of each blocking event. It is defined in analogy to (6) where just the individual duration $l_j$ has to be replaced by the constant $L$ (=7).

### b. *Results*

We have seen in the last section that the mountain effect produces a highly significant signal in the hemispheric mean wind balance. Therefore, let us first examine how the hemispheric mountain drag is related to blocking. Table 4 (upper part) gives the results for the cross-spectral analysis between $D(0, 90)$ and the three blocking indices $BL$, $B7$ and $BS$. In all three cases, one recognizes significant low-frequency coherencies ($f = 1/32$ and/or $f = 2/32$). The in-phase correlation between $BL$ and $D(0, 90)$ means that positive mountain drag anomalies prevail during the mature stage of blocking. On the other hand, we find a out-of-phase relation between $BS$, i.e., $B7$ and $D(0, 90)$. Because $BS$ and $B7$ have large amplitudes during the first blocking stage we conclude that we have an anomalously negative mountain drag before the onset, or at the very early stage, of a blocking episode.

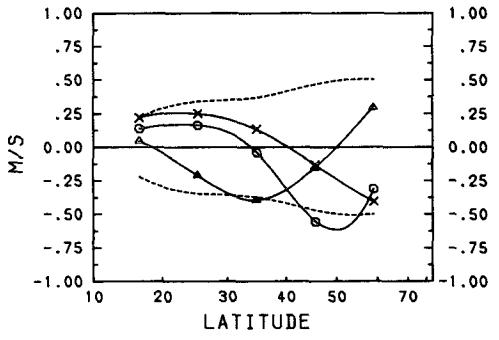


FIG. 8. The latitudinal distribution of sample averages of zonal mean wind anomalies for wintertime blocking (50 cases). Preblocking stage (triangles); first blocking phase (open circles); mature blocking stage (crosses). (See text.) Dashed curves represent 95% significance levels.

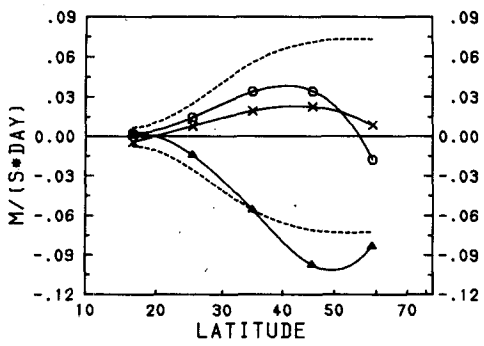


FIG. 9. As in Fig. 8 but for mountain drag anomalies.

Let us now look at the cross-spectrum of the latitude belt averages of the mountain drag and blocking. The squared coherency and phase spectrum for the blocking index *BS* is shown in Fig. 4. We find significant low-frequency coherencies at the three northern latitude belts (30°–40°), (40°–53°) and (53°–70°). At the same time the phase spectra exhibit a systematic decrease of the low-frequency phase estimates (1/32 and 2/32) with increasing latitude. One may verify that this phase shift reflects the fact that we have significant correlations between the mountain drag at different latitudes (cf. previous section). In terms of a correlation coefficient (Table 5) we have a positive correlation at a positive lag [$r(2) = 0.20$] at the belt (30°–40°). This points towards positive mountain drag anomalies during the first blocking phase. On the contrary, we have a negative correlation at negative lags at the latitudes 40–53° [$r(-6) = -0.24$], and 53°–70° [$r(-4) = -0.28$]. The correlations are significant with a 1% error probability. We found virtually the same result for the *B*7 index (not shown). Thus it appears that before the onset or at the very first stage of blocking a systematic negative mountain drag anomaly prevails at middle to high latitudes. The index *BL* exhibits significant coherencies only at the highest latitude belt (Fig. 5). The phase spectrum indicates a positive correlation for the mature blocking stage.

As a point of interest, let us discuss the relation between the zonal wind anomalies itself and blocking. The results for the superrotation $U(0, 90)$ are presented in the lower part of Table 4. Here, we have significant coherencies only for the *BS* index suggesting that we have to expect negative anomalies of the superrotation at the first stage of blocking. From the distribution of this correlation with latitude (Fig. 6, Table 5) we see that this effect is entirely due to the wind at the midlatitude belt 40°–53°. For that belt, a correlation coefficient of −0.56 at zero lag results. A similiar result is obtained for the index *B*7 (Fig. 7, upper panel). The mature stage index *BL* exhibits virtually no significant coherencies at the latitude belt 40°–53° (Fig. 7, lower panel).

To obtain an estimate of the magnitude of the anomalies during blocking we computed blocking sample mean values. Thereby, we subdivided each observed blocking episode into three stages; namely, a preblocking stage (days −7 to −1 before block started), a first-stage blocking period (days 0 to 6) and a mature stage period (days (7 to 13). The block starts were adopted from the catalogue of Treidl *et al.* (1981). Sample mean values over all winter blocks for the three blocking phases were evaluated for the latitude-belt mountain drag and wind anomalies. The latitudinal distribution of the blocking sample mean wind anomalies (Fig. 8) exhibits a significant negative anomaly of $-0.5$ m s$^{-1}$ only during the first stage of blocking and at the 40°–53° latitude band. Hartmann and Ghan (1980) found that the differences in the zonal mean 45°–65° latitude belt 500 mb zonal wind between blocks and transient ridges are $-1.2$ m s$^{-1}$ for the Pacific sector and $-1.8$ m s$^{-1}$ for the Atlantic sector. If one assumes that our anomalies correspond to one-half of the differences between blocks and transient ridges, our results compare most favorably with the values of Hartmann and Ghan. If we look at the mountain drag (Fig. 9), we find significant anomalies of $-0.1$ m s$^{-1}$/day at the 40°–53° and 53°–70° latitude belts for the preblocking stage. This finding agrees with the above described results of our cross-spectral analysis (Fig. 4).

## 5. Discussion

The results previously described indicate that the wintertime mountain drag is an important driving mechanism for the Northern Hemisphere barotropic wind. This is particularly true for the hemispheric average and the low-frequency components of the flow. At latitudes of the major mountain ranges (30°–40°) the mountain effect explains an appreciable fraction of the observed wind change. There are also significant coherencies between $D$(30°–40°) and the wind change in the adjacent 40–53° latitude belt. Apparently, the contributions from the 30°–40° latitudes also govern the hemispheric mean balance. At high latitudes (53°–70°) we have significant coherencies, too, but here the mountain drag exhibits a significant lead of some days over the wind change. It appears that at those latitudes the mountain drag has no direct influence on the zonally averaged wind.

So far, we have established that the mountain drag is an important mechanism for the "normal" zonal mean wind balance. As we have outlined, we assume as a first step that this holds also during blocking episodes alone. The results of the cross-spectral analyses between the blocking index and the zonal mean wind suggest a strong correlation between blocking and the wind anomalies at midlatitudes (40°–53°). In particular, during blocking negative wind anomalies occur most frequently at that latitude belt. The magnitude of these anomalies compare well with the results of Hartmann and Ghan (1980). Our analysis indicates that this midlatitude negative wind anomaly is most significant at the first stage of a blocking event. The

midlatitude belt anomalies also give significant negative anomalies in the superrotation $U(0, 90)$. We did not obtain significant results for the mature blocking stage (index *BL*).

We found, that before the onset of blocking the mountain drag exhibits highly significant negative anomalies at middle to high latitudes (40°–70°). This effect dominates the hemispheric mean as well. At the latitude belt of the main mountain ranges (30°–40°) positive anomalies appear to occur commonly during the first stage of blocking. The mature blocking stage seems to be characterized by significant positive mountain drag anomalies at high latitudes (53°–70°) and for the hemispheric mean, but no significant correlation appears at the 30°–40° latitude belt.

Finally, let us briefly comment on the steady state blocking theory (Charney and DeVore 1979). Charney *et al.* (1981) compared the steady state response of a Charney and DeVore type midlatitude channel-flow model with orographic forcing to zonal geopotential height profiles averaged over selected blocking cases. They found that the ridges of their blocking solutions were in reasonable agreement with the observations (cf. Shukla and Mo, 1983). With respect to the findings of the present paper, it will be interesting to examine the results of Charney *et al.* for the zonally averaged flow and mountain drag. The latter used the observed earth's topography, averaged over the latitudes 42°, 46° and 50°N. Thus it will be reasonable to compare their results with our 40–53° latitude belt analyses. The zonal flow applied by Charney *et al.* is the mean wind $U_0$ (averaged over the area of the channel). It is governed by (cf. Eq. (3) of Charney *et al.*):

$$dU_0/dt = D_0 + kU_0^* - kU_0. \tag{7}$$

Here $D_0$ is the channel mean value of the mountain drag. Equation (7) corresponds to the latitude average of (2) except that the surface stress is parameterized and the mean eddy boundary fluxes are replaced by the constant driving $kU_0^*$. Thus, at steady state (7) gives

$$D_0 = -k(U_0^* - U_0). \tag{8}$$

Charney *et al.* have matched the subresonant wavenumber 2 equilibrium to the normal January mean solution of Charney and Eliassen (1949). Let $U_{0N}$ denote this January mean wind. The blocking equilibria (wavenumber 3) are all characterized by a zonal mean wind $U_{0B} < U_{0N}$. This agrees with our findings that blocking episodes are characterized by significant negative wind anomalies at 40–53°. By virtue of (8) this implies $D_{0B} - D_{0N} < 0$. As already discussed, we found significant negative mountain drag anomalies at 40°–53°. So far, the agreement of Charney *et al.* with our analysis is quite good. However, some remaining points must be mentioned. First, our analysis suggests that the mountain drag anomalies occur before blocking starts. We did not obtain very significant results for the mature-stage blocking index. Second, we have shown that for climatological normal conditions (Fig. 2) the signal-to-noise ratio of the mountain drag at 40–53° is small (11% at periods of 64–21 days and 17% at periods of 21–12 days). Thus, if the blocking equilibrium of Charney *et al.* is associated with similar time scales there is no reason to assume that the mountain drag is so substantially stronger during blocking that it can balance the mean surface stress. On the other hand, the neglect of the mean vorticity boundary fluxes is an unavoidable feature of the model of Charney *et al.* Therefore, it would be highly desirable to reexamine the Charney and DeVore problem by applying a better parameterization of the time-mean eddy boundary momentum fluxes.

*Acknowledgments.* The author is grateful to two anonymous reviewers for their many helpful remarks and suggestions.

## APPENDIX

### Cross-spectral Techniques

Prior to the spectral analysis, the time series were detrended. We computed daily anomalies $X'(t)$ as deviations from the long-term climate ensemble.

$$X'(t) = X(t) - X^*(t). \tag{A1}$$

As defined, $X^*(t)$ is the normal annual cycle represented by the mean and the yearly and half-yearly Fourier component. The whole time series is split into individual seasons. In the present paper only the winter season (96 days, starting from 1 December) is considered. In addition, the mean and the linear trend for each winter are subtracted. Thus fluctuations due to interannual variability have been removed. Time derivatives are evaluated by applying a centered difference operator.

Cross-spectra were evaluated for the nine winters from 1967/68 to 1975/76. A segmented Fast Fourier technique (IMSL routine FTFPS, IMSL 1981) was used to compute the spectra. Thereby an elementary segment length of 32 days is applied, i.e., each winter is subdivided into three nonoverlapping subsegments. The nine winters lead to 27 subsegments so that each spectral estimate is based upon 54 degrees of freedom (dof). The spectrum is composed of 17 spectral estimates at frequencies $f_i = i/32$ cycles per day (cpd), $i = 0, 1, \ldots, 16$.

The squared coherence spectrum $K^2(f_i)$ and the phase spectrum $F(f_i)$ between the two time series $X(t)$ and $Y(t)$ are defined as

$$K^2(f_i) = \frac{L^2(f_i) + Q^2(f_i)}{P_x(f_i)P_y(f_i)} \tag{A2}$$

and

$$F(f_i) = \tan^{-1}[-Q(f_i)/L(f_i)] \tag{A3}$$

where $L(f_i)$, $Q(f_i)$, $P_x(f_i)$ and $P_y(f_i)$ are the cospectrum, quadrature spectrum, power spectrum of $X(t)$ and

power spectrum of $Y(t)$, respectively at frequency $f_i$ (cf. Jenkins and Watts 1968). The $K^2(f_i)$ takes values between 0 and 1 while the phase ranges from $-\pi$ to $\pi$. The phase spectrum shows whether the frequency components in the $Y(t)$ series lead $[F(f_i) > 0]$ or lag $[F(f_i) < 0]$ the components at the same frequency in the $X(t)$ series. The lagged covariance and the cross-spectrum are Fourier pairs. Thus the correlation coefficient $r_{xy}(l)$ at lag $l$ is given by

$$r_{xy}(l) = \frac{\int_0^\infty [L^2(f) + Q^2(f)]^{1/2} \cos[2\pi fl + F(f)]df}{\left[\int_0^\infty P_x(f)df \int_0^\infty P_y(f)df\right]^{1/2}}. \tag{A4}$$

In the present paper a discrete version of (A4) is applied (cf. also Jenkins and Watts, 1968). A "low-frequency" correlation coefficient is obtained by summing just over the spectral estimates at the frequencies $f_i = 1/32$, $2/32$ and $3/32$.

The significance of the squared coherence estimates is tested under the null-hypothesis of zero coherence by the statistic (Julian, 1975)

$$\beta = 1 - \alpha^{1/(\text{dof}/2-1)} \tag{A5}$$

where $\alpha$ is the error probability and *dof* is the number of degrees of freedom. A $(1 - \alpha)$ 100% confidence interval for the phase estimates is defined by (Koopmans, 1974)

$$F(f) - \gamma^* \leq \gamma \leq F(f) + \gamma^* \tag{A6}$$

where

$$\gamma^* = \sin^{-1}\langle\{[1 - K^2(f)]/[K^2(f)(\text{dof-}2)]\}^{1/2} t_{\text{dof-}2}(\alpha/2)\rangle.$$

Here $\gamma$ is the expected value of the phase and $t(\alpha/2)$ is the upper $\alpha/2$ cutoff point of the $t$-distribution with *dof-2* degrees of freedom.

## REFERENCES


Austin, J. F., 1980: The blocking of middle westerly winds by planetary waves. *Quart. J. Roy. Meteor. Soc.*, **108,** 327–350.

Baines, P. G., 1983: A survey of blocking mechanisms, with application to the Australian region. *Aust. Meteor. Mag.*, **31,** 27–36.

Branstator, G., 1984: The relationship between zonal mean flow and quasi-stationary waves in midtroposphere. *J. Atmos. Sci.*, **41,** 2163–2173.

Charney, J. G., and A. Eliassen, 1949: A numerical method for predicting the perturbations of the middle latitude westerlies. *Tellus,* **1,** 38–54.

——, and J. G. DeVore, 1979: Multiple flow equilibria in the atmosphere and blocking. *J. Atmos. Sci.*, **36,** 1205–1216.

——, J. Shukla and K. C. Mo, 1981: Comparison of a barotropic blocking theory with observations. *J. Atmos. Sci.*, **38,** 762–779.

Dole, R. M., 1982: Persistent anomalies of the extratropical northern hemisphere wintertime circulation. Ph.D. thesis, MIT, 225 pp.

Frederiksen, J. S., 1982: A unified three-dimensional instability theorie of the onset of blocking and cyclogenesis. *J. Atmos. Sci.*, **39,** 969–982.

Hansen A. R., and T.-C. Chen, 1982: A spectral energetics analysis of atmospheric blocking. *Mon. Wea. Rev.*, **110,** 1146–1165.

Hartjenstein, G., 1984: Observational evidence of the relations between large-scale orographic forcing, blocking and the stratospheric winter circulation. *Contrib. Atmos. Phys.*, **57,** 169–182.

Hartmann, D. L., and S. J. Ghan, 1980: A statistical study of the dynamics of blocking. *Mon. Wea. Rev.*, **108,** 1144–1159.

IMSL Library, 1981: Edition 8, IMSL Inc., Houston, Texas.

Jenkins, G. M., and D. G. Watts, 1968: *Spectral Analysis and its Applications,* Holden-Day, 525 pp.

Julian, P. R., 1975: Comments of the determination of significance levels on the coherence statistic. *J. Atmos. Sci.*, **32,** 836–837.

Källen, E., 1982: Bifurcation properties of quasi-geostrophic, barotropic models and their relation to atmospheric blocking. *Tellus,* **34,** 255–265.

Koopmans, L. H., 1974: *The Spectral Analysis of Time Series,* Academic Press, 366 pp.

Lorenz, E. N., 1979: Forced and free variations of weather and climate. *J. Atmos. Sci.*, **36,** 1367–1376.

Newton, C. W., 1971: Mountain torques in the global angular momentum balance. *J. Atmos. Sci.*, **28,** 623–628.

Oort, A. H., and H. D. Bowman, 1974: A study of the mountain torque and its interannual variations in the Northern Hemisphere. *J. Atmos. Sci.*, **31,** 1974–1982.

Shukla, J., and K. C. Mo, 1983: Seasonal and geographical variation of blocking. *Mon. Wea. Rev.*, **111,** 389–402.

Speth, P., and E. Kirk, 1981: Representation of meteorological fields by spherical harmonics. *Meteor. Rundsch.*, **34,** 5–10.

Schilling, H. D., 1985: On Atmospheric Blocking Types and Blocking Numbers, *Advances in Geophysics,* Academic Press,

Treidl, R. A., E. C. Birch and P. Sajecki, 1981: Blocking action in the northern hemisphere: A climatological study. *Atmos.-Ocean,* **19,** 1–23.

Tung, K. K., and R. S. Lindzen, 1979: A theory of stationary long waves. Part I: A simple theory of blocking. *Mon. Wea. Rev.*, **107,** 714–734.

White, R. M., 1949: The role of mountains in the angular momentum balance of the atmosphere. *J. Meteor.*, **6,** 353–355.

White, W. B., and N. E. Clark, 1975: On the development of blocking ridge activity over the central North Pacific. *J. Atmos. Sci.*, **32,** 489–502.